

Dynamical description of the breakup of one-neutron halo nuclei ^{11}Be and ^{19}C

S. Typel¹ and R. Shyam^{1,2}

¹*National Superconducting Cyclotron Laboratory, Michigan State University, East Lansing,
Michigan 48824-1321, U.S.A.*

²*Saha Institute of Nuclear Physics, Calcutta 700064, India*
(November 5, 2018)

We investigate the breakup of the one-neutron halo nuclei ^{11}Be and ^{19}C within a dynamical model of the continuum excitation of the projectile. The time evolution of the projectile in coordinate space is described by solving the three-dimensional time dependent Schrödinger equation, treating the projectile-target (both Coulomb and nuclear) interaction as a time dependent external perturbation. The pure Coulomb breakup dominates the relative energy spectra of the fragments in the peak region, while the nuclear breakup is important at higher relative energies. The coherent sum of the two contributions provides a good overall description of the experimental spectra. Cross sections of the first order perturbation theory are derived as a limit of our dynamical model. The dynamical effects are found to be of the order of 10-15% for the beam energies in the range of 60 - 80 MeV/nucleon. A comparison of our results with those of a post form distorted wave Born approximation shows that the magnitudes of the higher order effects are dependent on the theoretical model.

PACS numbers: 24.10.Eq., 25.60.-t, 25.60.Gc, 24.50.+g

KEYWORD: Coulomb and nuclear breakup, time dependent Schrödinger equation, finite range DWBA and first order perturbation theory

I. INTRODUCTION

^{11}Be and ^{19}C are examples of one-neutron halo nuclei, where the loosely bound valence neutron has a large spatial extension with respect to the respective cores (see, e.g., [1–3] for a recent review). Breakup reactions, in which the valence neutron is removed from the projectile in its interaction with a target nucleus, have played a very useful role in probing the structure of such nuclei [4–10]. Strongly forward peaked angular distributions for the neutron [11,12] and the narrow widths of the parallel momentum distributions [13–19] of the core fragments are some of the characteristic features of the breakup reactions induced by these nuclei, which provide a clean confirmation of their halo structure. In the Serber types of models [18,20], the breakup cross section is directly related to the momentum space wave function of the projectile ground state.

The Coulomb breakup is a significant reaction channel in the scattering of halo nuclei from a heavy target nucleus (see, e.g., [21]). It provides a convenient way to put constraints on the electric dipole response of these nuclei [22,23]. The Coulomb breakup of weakly bound nuclei can also be used in determining the cross sections of the astrophysically interesting radiative capture reactions [24].

The breakup of the halo nuclei have been investigated theoretically by several authors using a number of different approaches (see, e.g., [10] for an extensive list of references). Some of these models [18,25,26] use semiclassical geometrical concepts (mostly Serber type) to calculate the breakup cross sections. A direct breakup model (DBM) (which reduces to the Serber model in a particular limit [27]) has been formulated within the framework of the post form distorted wave Born approximation (DWBA) [28,10]. However so far only the Coulomb breakup of the halo nuclei has been investigated within this theory. The nuclear breakup, for these cases, has been studied mostly within the semiclassical [29] and eikonal models [30,31].

Breakup reactions of halo nuclei can also be described as the inelastic excitation of the projectile from its ground state to the continuum [32,33]. In an extensively used theoretical approach, the corresponding T-matrix is written in terms of the prior form DWBA [28]. For the pure Coulomb breakup, the semiclassical approximation of this theory is the first order perturbative Alder-Winther theory of Coulomb excitation [34]. It has recently been used to analyze the data on the breakup reactions induced by ^{11}Be [8] and ^{19}C [9]. However, higher order excitation effects [35–39] may be substantial in the breakup of these nuclei. It has been shown [10,40] that for the Coulomb breakup of ^{19}C , the results of the first order semiclassical Coulomb excitation theory differ strongly from those of the DBM which includes the higher order effects.

The general methods in the semiclassical description of the excitation process which include higher order effects, are the coupled channel approaches [41], explicit inclusion of successive higher order terms [42], and the direct numerical integration of the time dependent Schrödinger equation [36–38,43]. The last method, in which all the higher order effects in the relative motion of the breakup fragments are included, provides a fully dynamical calculation of the projectile excitation caused by both the Coulomb and the nuclear interactions between the projectile and the target.

The time dependent Schrödinger equation method has been used earlier [36,37] to investigate the Coulomb breakup of ^{11}Li and ^{11}Be . However, these calculations have employed

a straight line trajectory for the projectile motion (an approximation valid at higher beam energies) and have ignored the spins of the particles in the nuclear models. Furthermore, they are partly perturbative in the sense that the first order perturbation theory has been used therein to calculate the energy distribution of the breakup cross section at larger impact parameters. This procedure may lead [38] to a significantly larger cross section as compared to that obtained in models where the partly perturbative approximation is not used.

In this paper, we present calculations for both the Coulomb and the nuclear breakup of the one-neutron halo nuclei ^{11}Be and ^{19}C within the time dependent Schrödinger equation method (this will be referred as the dynamical calculation in the rest of this paper). The spins of the particles are included explicitly in the nuclear model. The Hamiltonian describing the internal motion of the projectile contains a spin dependent interaction. No perturbative approximation has been made in the calculation of the breakup cross sections. We also calculate first order perturbative results as a limit of our dynamical model so that a consistent investigation of the role of the dynamical effect in the breakup cross sections is possible. We compare the results of our calculations with those of the post form finite range DWBA theory to study the magnitudes of the higher order effects calculated in different approaches.

Our manuscript is organized in the following way. In section II, we give the details of our formalism. The comparison of our calculations with the experimental data and the discussion of the results are presented in section III. The summary and conclusions of our paper are given in section IV.

II. FORMALISM

In this section, we describe a general method for solving the time dependent Schrödinger equation, which can be used in problems depending upon a single three-dimensional dynamical variable. The potentials involved are assumed to be local. The time development of the wave function of the relative motion between the neutron and the core nucleus, $[\Psi(\mathbf{r}, t)]$, is given by the time dependent Schrödinger equation

$$i\hbar\frac{\partial}{\partial t}\Psi(\mathbf{r}, t) = [H_0(\mathbf{r}) + V(\mathbf{r}, t)]\Psi(\mathbf{r}, t), \quad (1)$$

where $H_0(\mathbf{r})$ is the internal Hamiltonian describing the relative motion between the valence neutron (n) and the core nucleus (b). It is defined as

$$H_0(\mathbf{r}, t) = -\frac{\hbar^2}{2\mu_{bn}}\Delta + V_0(\mathbf{r}), \quad (2)$$

where μ_{bn} is the reduced mass of the $n + b$ system and $\mathbf{r} = \mathbf{r}_n - \mathbf{r}_b$. The potential $V_0(\mathbf{r})$ could contain a central and a spin-orbit term. In Eq. (1), $V(\mathbf{r}, t)$ is the time dependent external field exerted by the target on the projectile. In the present application, it is the Coulomb and nuclear interaction between the target (A) and the projectile (a). We write

$$\Psi(\mathbf{r}, t) = \sum_c \frac{\psi_c(r, t)}{r} \mathcal{Y}_{J_c M_c}^{\ell_c}(\hat{\mathbf{r}}), \quad (3)$$

with

$$\mathcal{Y}_{J_c M_c}^{\ell_c}(\hat{\mathbf{r}}) = \sum_{m_\ell m_s} (\ell_c m_\ell s m_s | J_c M_c) Y_{\ell_c m_\ell}(\hat{\mathbf{r}}) \chi_{s m_s}, \quad (4)$$

where c stands for the individual channels characterized by the quantum numbers J_c , M_c , and ℓ_c . The orbital angular momentum (ℓ_c) is coupled to the neutron spin ($s = \frac{1}{2}$) to give the total angular momentum (J_c) under the assumption of zero spin for the core nucleus. Substituting Eqs. (2) and (3) into Eq. (1), we can write a set of coupled equations for the radial wave function

$$i\hbar \frac{\partial}{\partial t} \psi_{c'}(r, t) = \sum_c h_{c'c}(r, t) \psi_c(r, t), \quad (5)$$

where

$$h_{cc'}(r, t) = \left[-\frac{\hbar^2}{2\mu_{bn}} \left(\frac{\partial^2}{\partial r^2} - \frac{\ell_c(\ell_c + 1)}{r^2} \right) + V_0^c(r) \right] \delta_{cc'} + V^{cc'}(r, t). \quad (6)$$

The solution of the radial equation (5) can be written as

$$\psi_c(r, t) = \psi_c(r, t_i) + \frac{1}{i\hbar} \int_{t_i}^t dt' \sum_{c'} h_{cc'}(r, t') \psi_{c'}(r, t'), \quad (7)$$

with the starting time t_i . Alternatively, the wave function at time t can be calculated from the initial wave function by applying the unitary time evolution operator (in the obvious matrix notation)

$$\psi(t) = \mathbf{U}(t_i, t) \psi(t_i). \quad (8)$$

For a small time step Δt , the time evolution operator can be approximated as

$$\mathbf{U}(t, t + \Delta t) \approx \frac{\mathbf{1} + \frac{\Delta t}{2i\hbar} \mathbf{h}(t)}{\mathbf{1} - \frac{\Delta t}{2i\hbar} \mathbf{h}(t)}, \quad (9)$$

where the elements of the matrix \mathbf{h} are given by $h_{cc'}$. Eqs. (8) and (9) are the starting points for the numerical solution of the problem, which has been done by following the method described in Ref. [43]. This approach has the virtue that a first order calculation can also be performed within the same program by keeping the coupling only between the initial channel ($c' = c_{in}$) and all the possible final channels (c) in the perturbation potential, i.e., by replacing $V^{cc'}$ by $V^{cc'} \delta_{c'c_{in}}$ in Eq. (6). Then the matrix \mathbf{h} is no longer hermitian and the time evolution operator \mathbf{U} becomes non-unitary.

Unlike the previous calculations [36–38], we do not assume the projectile to move on a straight line trajectory. In our case, the c.m. of the projectile is supposed to follow a hyperbolic trajectory with respect to the target during the scattering process. For application to the breakup of the one-neutron halo nuclei, the Coulomb part of the external perturbation [$V_C(\mathbf{r}, t)$] is given by

$$V_C(\mathbf{r}, t) = \frac{Z_A Z_b e^2}{|\mathbf{r}_b - \mathbf{R}_A(t)|} - \frac{Z_A Z_b e^2}{|\mathbf{R}_A(t)|}, \quad (10)$$

where Z_A and Z_b are the charge numbers of the target and the core nuclei, respectively. $\mathbf{R}_A(t)$ is the coordinate of the target in the projectile centre of mass (c.m.) frame, and $\mathbf{r}_b = -\frac{m_n}{m_n+m_b}\mathbf{r}$ and $\mathbf{r}_n = \frac{m_b}{m_n+m_b}\mathbf{r}$, are the position vectors of the core nucleus and the neutron, respectively. The nuclear part of the external perturbation $[V_N(\mathbf{r}, t)]$ is the sum of the neutron-target and core-target optical model potentials, respectively. It is given by

$$V_N(\mathbf{r}, t) = V_n f(|\mathbf{r}_n - \mathbf{R}_A(t)|, R_{Vn}, a_{Vn}) + iW_n f(|\mathbf{r}_n - \mathbf{R}_A(t)|, R_{Wn}, a_{Wn}) \\ + V_b f(|\mathbf{r}_b - \mathbf{R}_A(t)|, R_{Vb}, a_{Vb}) + iW_b f(|\mathbf{r}_b - \mathbf{R}_A(t)|, R_{Wb}, a_{Wb}), \quad (11)$$

where

$$f(x, R, a) = \left[1 + \exp\left(\frac{x-R}{a}\right) \right]^{-1} \quad (12)$$

with the diffuseness parameter a and radius R . The depths of the real and the imaginary parts of the neutron-target and the core-target optical potentials are denoted by V_n , W_n , and V_b , W_b , respectively. The corresponding radii and the diffuseness parameters are given by R_{Vn} , R_{Wn} , and a_{Vn} , a_{Wn} , and R_{Vb} , R_{Wb} and a_{Vb} , a_{Wb} , respectively.

Using a multipole expansion of the perturbation potentials, we can write

$$V^{cc'}(r, t) = \sum_{\lambda\mu} C_{cc'}^{\lambda\mu} \left[v_C^{\lambda\mu}(r, t) + v_N^{\lambda\mu}(r, t) \right], \quad (13)$$

with the coefficients

$$C_{cc'}^{\lambda\mu} = \int d\Omega \left[\mathcal{Y}_{J_c M_c}^{\ell_c} \right]^\dagger Y_{\lambda\mu} \mathcal{Y}_{J_{c'} M_{c'}}^{\ell_{c'}}. \quad (14)$$

The time dependent radial potentials are given by

$$v_C^{\lambda\mu}(r, t) = \frac{4\pi Z_A Z_b e^2}{2\lambda + 1} \left(\frac{-m_n}{m_n + m_b} \right)^\lambda \frac{r^\lambda}{R_A^{\lambda+1}(t)} Y_{\lambda\mu}^*(\hat{\mathbf{R}}_A(t)) \quad (15)$$

and

$$v_N^{\lambda\mu}(r, t) = V_n f^{\lambda\mu}(r_n, R_{Vn}, a_{Vn}, t) + iW_n f^{\lambda\mu}(r_n, R_{Wn}, a_{Wn}, t) \\ + V_b f^{\lambda\mu}(r_b, R_{Vb}, a_{Vb}, t) + iW_b f^{\lambda\mu}(r_b, R_{Wb}, a_{Wb}, t), \quad (16)$$

where

$$f^{\lambda\mu}(r, R, a, t) = \int d\Omega f(|\mathbf{r} - \mathbf{R}_A(t)|, R, a) Y_{\lambda\mu}^*(\hat{\mathbf{r}}). \quad (17)$$

The triple differential cross section for the breakup of the projectile a into b and n is given by

$$\frac{d^3\sigma}{dE_{bn} d\Omega_{bn} d\Omega_{bn-A}} = \frac{d\sigma_R}{d\Omega_{bn-A}} P_{if}(\mathbf{k}_{bn}) \rho_f(k_{bn}), \quad (18)$$

where Ω_{bn-A} are the angles associated with the relative motion of the c.m. of the $b+n$ system with respect to the target nucleus A . The first term on the right hand side of Eq. (18) is the Rutherford cross section for the projectile-target scattering. The last term,

$$\rho_f = \frac{\mu_{bn} k_{bn}}{(2\pi)^3 \hbar^2}, \quad (19)$$

is the density of final states. The excitation probability, P_{if} (which is a function the relative momentum $\hbar \mathbf{k}_{bn}$ between the two fragments), is given by

$$P_{if}(\mathbf{k}_{bn}) = \lim_{t_f \rightarrow \infty} \frac{1}{2J_i + 1} \sum_{M_i m_s} \left| \langle \Phi_{m_s}^{(-)}(\mathbf{k}_{bn}, \mathbf{r}) | \Psi_{M_i}(\mathbf{r}, t_f) \rangle \right|^2, \quad (20)$$

where $\Phi_{m_s}^{(-)}(\mathbf{k}_{bn}, \mathbf{r})$ is a complete scattering solution for the relative motion of the two fragments with the in-going wave boundary condition. It satisfies the Schrödinger equation (1) for a vanishing perturbation potential $V(\mathbf{r}, t)$. The wave function $\Psi_{M_i}(\mathbf{r}, t_f)$ is the solution of the time-dependent Schrödinger equation with the boundary condition that as $t_i \rightarrow -\infty$, it goes to the unperturbed wave function Φ_{M_i} of the ground state of the projectile. Since we are interested only in the breakup contributions, it is advantageous for numerical reasons to replace the full wave function $\Psi_{M_i}(\mathbf{r}, t)$, in Eq. (20), by the corresponding continuum wave function

$$\Psi_{M_i}^{\text{cont}}(\mathbf{r}, t) = \Psi_{M_i}(\mathbf{r}, t) - \sum_{b'} \langle \Phi_{b'}(\mathbf{r}, t) | \Psi_{M_i}(\mathbf{r}, t) \rangle \Phi_{b'}(\mathbf{r}, t), \quad (21)$$

where the sum runs over all bound states of the system.

In the actual numerical realization, the radial wave functions $\psi_c(r, t)$ are discretized on a mesh with points $x_n = n\Delta x$ where $\Delta x = 0.0025$ and $n = 0, \dots, 400$. They are related to the points in the radial coordinate r by the mapping, $r_n = R_{max}[\exp(ax_n) - 1]/[\exp(a) - 1]$, with $R_{max} = 900$ fm. The parameter a is chosen so that $r_1 = 0.3$ fm. The second order derivative, $\frac{\partial^2}{\partial r^2}$, in Eq. (6) is represented by a finite difference approximation. In the first step, the ground state radial wave function is calculated assuming a Woods-Saxon potential, $V_0^c(r) = V_0 f(r, R_0, a_0) \delta_{cc'}$, for the $n - b$ interaction in the initial channel with a given set of quantum numbers, J_c , M_c , and ℓ_c . The time evolution of this initial wave function is calculated by the repeated application of the time evolution operator (9), using time steps $\Delta t = 1$ fm/c, and taking into account partial waves with $\ell = 0, 1, 2, 3$ for the $n - b$ relative motion. This leads to a set of coupled linear equations for the radial wave functions which are solved with the technique as described in Ref. [43]. We use a time interval for the evolution which is symmetric to the time of closest approach between the target and the projectile. Its limits are determined by the condition that the perturbation potential is at least 200 times smaller than its maximum value. In order to avoid spurious excitations, the time dependent potential was switched on adiabatically. Furthermore, care has been taken to ensure that unphysical bound states are not populated during the time evolution.

TABLE I. Optical potential parameters for the neutron-target and core-target interaction.

projectile	V_n [fm]	R_{Vn} [fm]	a_{Vn} [fm]	W_n [fm]	R_{Wn} [fm]	a_{Wn} [fm]	Ref.
^{11}B	-27.88	6.93	0.75	-14.28	7.47	0.58	[51]
^{19}C	-29.48	6.93	0.75	-13.18	7.47	0.58	[51]
projectile	V_b [fm]	R_{Vb} [fm]	a_{Vb} [fm]	W_b [fm]	R_{Wb} [fm]	a_{Wb} [fm]	Ref.
^{11}Be	-70.0	5.45	1.04	-58.9	5.27	0.887	[52]
^{19}C	-200.0	5.39	0.90	-76.2	6.58	0.38	[53]

The final wave function is projected onto scattering states and the excitation probability is calculated according to Eq. (20), after removing the bound state contributions. For each M_c substate of the initial state, an independent calculation has been performed.

III. RESULTS AND DISCUSSIONS

The parameters of the nuclear optical potentials for the n -target and core-target interaction [see, Eq. (16)] used in our calculations, are given in Table I. We have adopted a single particle potential model to calculate the ground state wave function of the projectile. The ground state of ^{11}Be was assumed to have a $2s_{1/2}$ valence neutron coupled to the 0^+ ^{10}Be core with a binding energy of 504 keV. The corresponding single particle wave function was constructed by assuming the neutron - ^{10}Be interaction of the Woods - Saxon type having a central and a spin-orbit part. The radius and the diffuseness parameters in both the terms were taken to be 2.478 fm and 0.5 fm, respectively. The depth of the central term was searched so as to reproduce the ground state binding energy. This $2s_{1/2}$ wave function has an additional node as compared to a simpler zero-range wave function. The strength of the spin-orbit term was adjusted by requiring that the first excited ($\frac{1}{2}^-$) state in ^{11}Be is at the experimental excitation energy of 320 keV. In the dynamical calculation, we assume a vanishing n -core potential for the higher partial waves so that unphysical resonances can be avoided. For ^{19}C , the ground state wave function was obtained with the similar procedure by assuming a configuration in which a $2s_{1/2}$ neutron is coupled to the 0^+ ^{18}C core. The radius and the diffuseness parameters associated with the Woods-Saxon interaction were taken to be 3.30 fm and 0.65 fm, respectively. In the dynamical calculations, we took into account only the n -core interaction in the s-wave. The spectroscopic factors for the ground

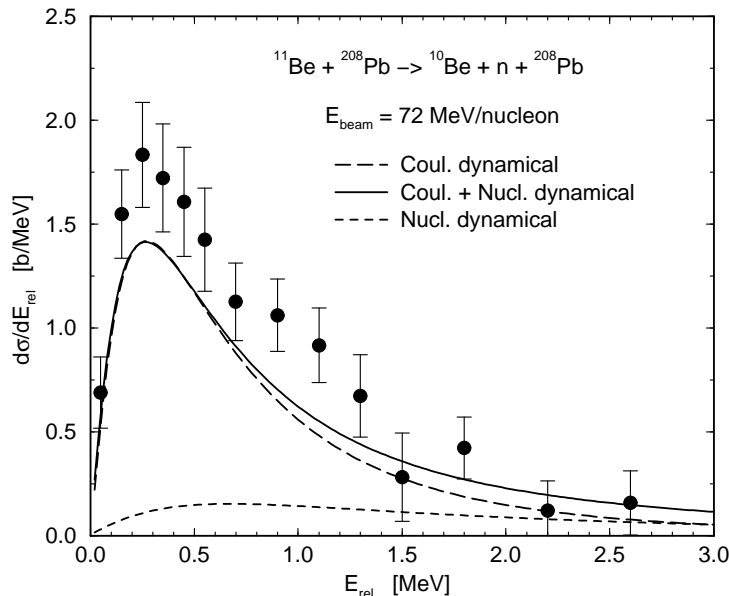


FIG. 1. The differential cross section as a function of the relative energy of the fragments (neutron and ^{10}Be) emitted in the ^{11}Be induced breakup reaction on a ^{208}Pb target at the beam energy of 72 MeV/nucleon. The long-dashed and short-dashed lines represent the pure Coulomb and pure nuclear breakup contributions, respectively. Their coherent sum is depicted by the solid line. The experimental data are taken from [8].

state were taken to be 1 in all the cases. In the multipole expansion of the perturbation potential [Eq. (13)], we included contributions up to $\lambda = 2$.

In Fig. 1, we compare the results of our calculations with the experimental data (taken from [8]) for the relative energy spectrum of the fragments emitted in the breakup reaction of ^{11}Be on a ^{208}Pb target at the beam energy of 72 MeV/nucleon. In these calculations, the integration over the theta (θ_{bn-A}) angles of the projectile c.m. was done in the range of $0^\circ - 3^\circ$, which corresponds to a minimum impact parameter of about 12 fm. The long-dashed and short-dashed lines represent the results of the dynamical calculations for the pure Coulomb and the pure nuclear breakup, respectively, while their coherent sum is represented by the solid line. The Coulomb cross sections consist mostly of the dipole term as the contributions of the quadrupole mode are negligible.

We note that the pure Coulomb contributions dominate the cross sections around the peak value while the nuclear breakup is important at the larger relative energies. This can be understood from the energy dependence of the two contributions. The nuclear breakup occurs when the projectile and the target nuclei are close to each other. Its magnitude which is determined mostly by the geometrical conditions, has a weak dependence on the relative energy of the outgoing fragments beyond a certain minimum value. Contrary to this, the Coulomb breakup contribution has a long range and it shows a strong energy dependence. The number of virtual photons increases for small excitation energies. At the same time, a much larger range in the impact parameter implies a substantial breakup probability. The results shown in this figure are in agreement with those of Ref. [44]. The domination of the nuclear breakup may explain the failure of the pure Coulomb finite range DWBA calculations [10] in explaining the data at larger relative energies.

The coherent sum of the Coulomb and the nuclear contributions provides a good overall description of the experimental data. Although, the pure nuclear breakup contributions below 0.5 MeV are substantial, yet their interference with the Coulomb part does not change appreciably the shape of the total cross section in the peak region. It may be noted that the absolute magnitude of the cross section near the maximum is somewhat underestimated by our calculations, but the position of the peak is well reproduced. This is in agreement with the results of the dynamical calculations reported in [38]. However, in the semiclassical coupled-channel calculations [44] for this reaction, the peak position of the calculated cross sections are shifted towards larger energies as compared to that of the data.

It may be remarked that use of a some what smaller minimum impact parameter in the angular integration over the ^{11}Be c.m. would increase the cross sections which may reduce the difference between the experiment and the theory. However, this would mainly affect the nuclear contribution since it is more sensitive to the smaller projectile-target distances. The Coulomb contributions arise mostly from the much larger impact parameters as long as the excitation energy is not too large. At very small impact parameters the absorption due to the imaginary parts of the optical potentials will result in an effective cutoff. Since the optical potentials are not sufficiently well known, the choice of the maximum scattering angle introduces an uncertainty but our choice for this is a reasonable one.

In Fig. 2, we show the results of our dynamical calculations for the relative energy spectrum of the fragments (neutron and ^{18}C) emitted in the breakup of ^{19}C on a ^{208}Pb target at the beam energy of 67 MeV/nucleon. The integrations over θ_{bn-A} were done in the range of $0^\circ - 3^\circ$. Since the binding energy (B_{n-core}) of the valence neutron - core system

in the ground state of ^{19}C is still an unsettled issue [21,46–49], we present in this figure the results of calculations performed with two values [530 keV (part a) and 650 keV (part b)] of $B_{n\text{-core}}$. This is for the first time that the dynamical calculations (including the nuclear breakup) have been performed for this case. The experimental data are taken from [9]. We see that the Coulomb breakup dominates the cross sections in the peak region while the nuclear breakup is important at the larger relative energies in this case too.

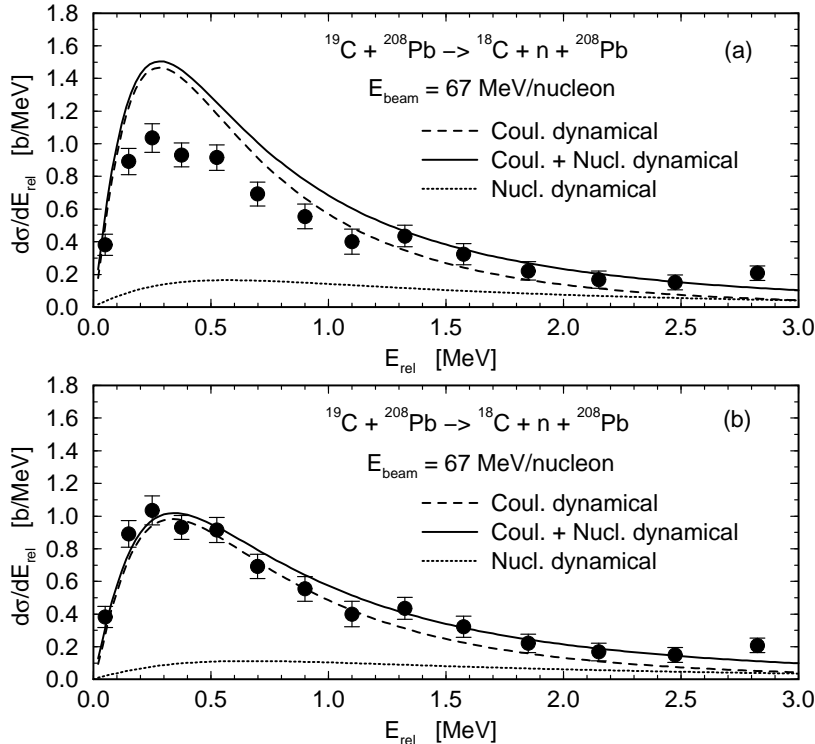


FIG. 2. The relative energy spectrum of the fragments (neutron and ^{18}C) in the breakup of ^{19}C on a ^{208}Pb target at the beam energy of 67 MeV/nucleon. Part (a) shows the results obtained with a binding energy of 530 keV for the neutron-core configuration in the ground state of ^{19}C while part (b) is the result with a value of 650 keV for the same. The dashed and dotted lines represent the pure Coulomb and pure nuclear breakup contributions, respectively, while their coherent sum is shown by the solid line. The experimental data are taken from [9].

The dynamical calculations carried out with the binding energy of 530 keV [part (a)] overestimate the cross sections in the peak region by about 35 - 40%, while those done with 650 keV [part (b)] are in good agreement with the data. Our calculations, therefore, seem to support the latter value for $B_{n\text{-core}}$ which is within the error range of the value [(530 ± 130) keV] reported in [9]. The expected shift in the peak position in part (b) is within statistical error of the data. We would like to recall, however, that we have used a spectroscopic factor of 1 for the neutron-core configuration for the ground state of ^{19}C .

An alternative scenario has been presented in [9], where the same data have been analyzed within the first order semiclassical perturbation theory of the Coulomb excitation. With a binding energy of 530 keV and the same neutron-core configuration for the ground state of ^{19}C , these calculations overestimate the data in the peak region by about 40-50% (see also [40]). Instead of using a larger value of $B_{n\text{-core}}$ in order to fit the data, these authors try to

extract a spectroscopic factor (SF) for this configuration by comparing their pure Coulomb dissociation calculations with the data (which are corrected for the nuclear breakup effects in an approximate way). The value of SF (0.67) obtained in this way is close to the shell model results of Ref. [45].

However, a note of caution must be added about the significance to this result. The spectroscopic factors reported in [45] correspond to various specific states of the ^{18}C core. The data of Ref. [9] are, however, inclusive in the sense that the specific core states of ^{18}C are not observed there. Therefore, measurements of the relative energy spectra in experiments of the type reported in [46], where specific core states of ^{18}C are identified by tagging to the decay photons, are required for a meaningful comparison of the SF extracted from such studies with those of the shell model. Moreover, the procedure adopted in [9] to correct the data for the nuclear breakup effects may not be valid due to the long range of the nuclear interaction in case of the halo nuclei [44]. Obviously, the value of the SF extracted from the breakup studies depends critically on the theory used to calculate the corresponding cross sections. Therefore, more experimental data and their theoretical analysis within different models of the breakup reactions are required for arriving at a more definite conclusion in this regard.

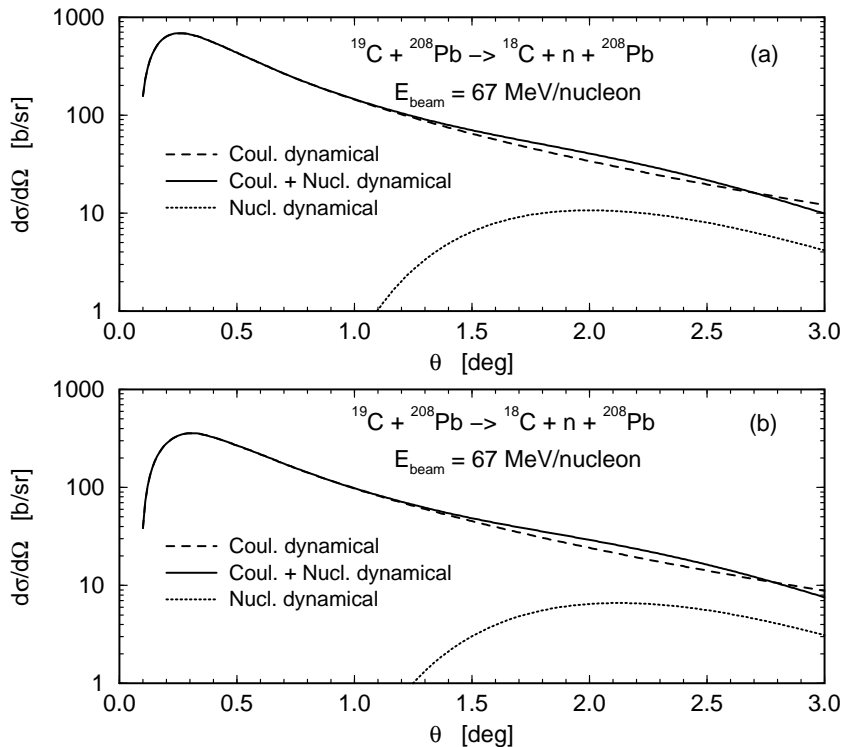


FIG. 3. Dynamical model results for the angular distribution of the center of mass of $n + ^{18}\text{C}$ system in the breakup of ^{19}C on a Pb target at the beam energy of 67 MeV/nucleon for two values [530 keV (part a) and 650 keV (part b)] of the ^{19}C ground state. The dashed and dotted lines represent the pure Coulomb and pure nuclear contributions. Their coherent sum is represented by the solid line.

Another argument put forward in [9] in favor of their procedure is that with the values 0.530 MeV and 0.67 for $B_{n\text{-core}}$ and SF, respectively, the angular distribution of the $n + ^{18}\text{C}$

c.m. measured in the same reaction is well reproduced. However, this conclusion assumes that the shape of this angular distribution is not affected by the nuclear breakup effects below the grazing angle ($\sim 2.7^\circ$). To study the role of the nuclear breakup for this data, we show in Fig. 3 the angular distribution of the c.m. of the $n + {}^{18}\text{C}$ system for the values of $B_{n\text{-core}}$ of 530 keV (upper part) and 650 keV (lower part). The integrations over the relative energy is performed in the range of 0.0–0.5 MeV (the same as done in Ref. [9]). It is clear from this figure that the nuclear breakup effects start becoming important already from c.m. angles of 1.5° , and the total cross section (coherent sum of the Coulomb and nuclear contributions) differs from the pure Coulomb one even below the grazing angle. Beyond this angle, the absorptive part of the optical potentials reduces the cross section. In this figure we have not shown the comparison of our calculations with the experimental data as it would require folding the calculations with the experimental angular resolution [9]. However, the comparison of the unfolded and folded results as shown in [40] suggests that the quality of agreement between calculations done with both the options and the data would be similar.

The magnitude of higher order effects in the Coulomb breakup reactions of ${}^{11}\text{Be}$ and ${}^{19}\text{C}$ is a subject of current interest. In an earlier calculation [36], higher order effects were found to be rather small for the reaction studied in Fig. 1. However, comparing the result of the adiabatic model of Coulomb breakup reactions with that of the first order semiclassical perturbation theory of the Coulomb excitation, it has been concluded in [39] that the higher order effects are substantial for the reaction investigated in Fig. 2, which

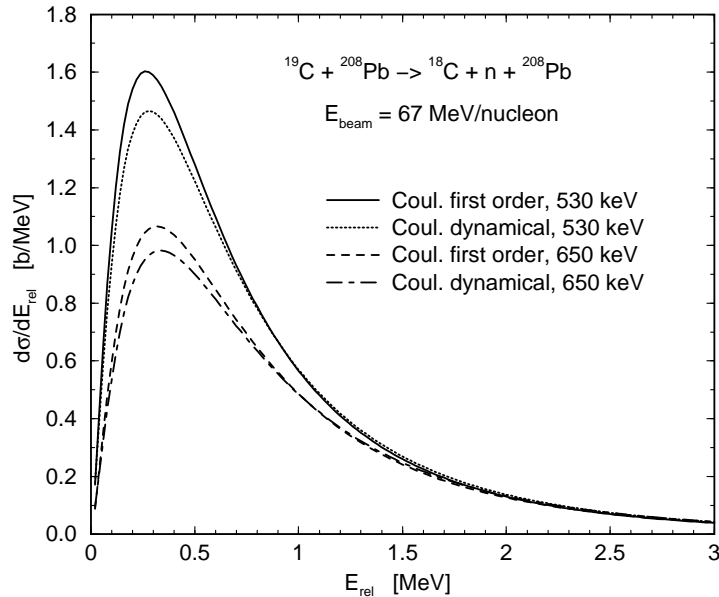


FIG. 4. Comparison of the dynamical model and the first order perturbation theory results for the pure Coulomb breakup contribution to the relative energy spectrum of the fragments (neutron and ${}^{18}\text{C}$) emitted in the breakup of ${}^{19}\text{C}$ on a ${}^{208}\text{Pb}$ target at the beam energy of 67 MeV/nucleon. The solid and dotted lines represent the results of the first order and the dynamical model calculations, respectively, obtained with the value of $B_{n\text{-core}}$ equal to 530 keV while the dashed and dashed-dotted lines represent the same for the $B_{n\text{-core}}$ value of 650 keV. The first order perturbation theory results have been obtained from the dynamical model in a particular limit as discussed in section II.

would have a considerable influence on the extracted spectroscopic factor. In contrast, these effects were found to be rather small in [50] where the first order and the higher order terms were calculated within the same model. As discussed in section II, the first order perturbation theory results can be obtained from our dynamical model in a particular limit. In Fig. 4, the first order results obtained in this way are compared with those of the full dynamical model for the pure Coulomb breakup contribution to the same reaction as in Fig. 2. It can be noted that the higher order effects are rather small. They reduce the peak cross sections of the first order theory by about 10% for both values of B_{n-core} but leave the shapes of the spectra largely unaffected.

In Fig. 5, we compare the pure Coulomb breakup contributions (calculated within the dynamical model and the finite range DWBA [10]) to the reactions studied in Figs. 1 and 2. In the finite range DWBA theory the higher order effects in the target-fragment interaction are automatically incorporated. The interesting aspect of this comparison is that while for the ^{11}Be case the finite range DWBA results are slightly larger than those of the dynamical semiclassical calculation, the former is smaller than the latter for ^{19}C induced reaction for both the values of the binding energy. This clearly shows that higher order calculations for the Coulomb breakup performed within different theories could be different from each other. The reason for this difference is the fact that fully quantal higher order approaches

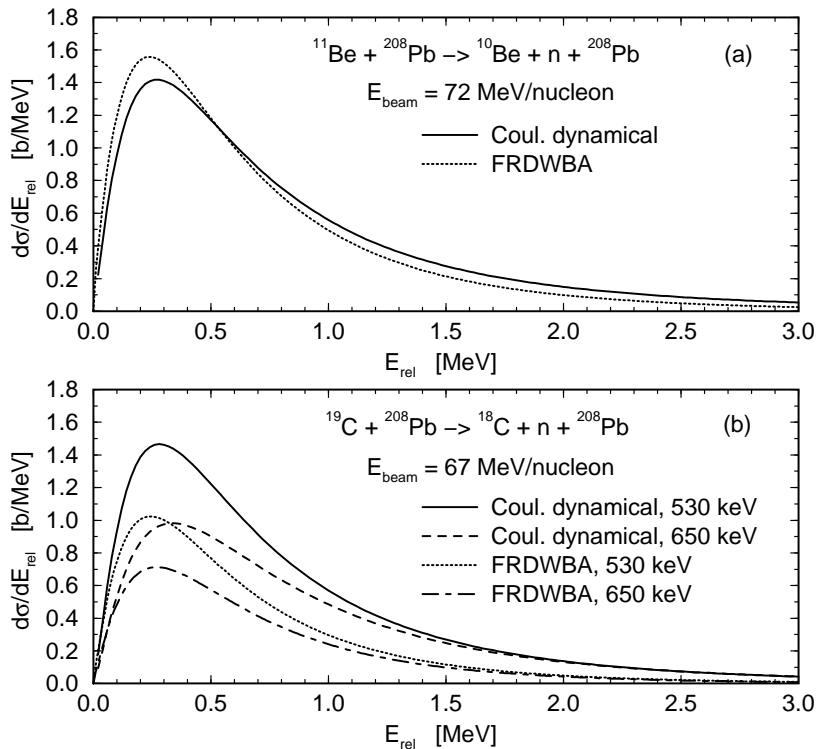


FIG. 5. (a) Comparison of the pure Coulomb dynamical model (solid line) and the finite range DWBA (dotted line) contributions to the relative energy spectrum of the fragments (neutron and the core) emitted in the pure Coulomb breakup of ^{11}Be on a ^{208}Pb target at the beam energy of 72 MeV/nucleon. (b) The same as in part (a) for the breakup of ^{19}C on the same target at the beam energy of 67 MeV/nucleon. In this case the full and dashed lines represent the results of the the dynamical model and finite range DWBA, respectively, corresponding the ^{19}C binding energy of 530 keV while dashed and dashed-dotted lines show the same for the binding energy of 650 keV.

take into account effects which are beyond the semiclassical dynamical model calculations. Therefore, the results of the semiclassical first order perturbation theory will differ from those of different higher order models in different ways. Thus, the conclusion about the role of the higher order effects will differ if the first order and higher order calculations performed within two different theories are compared with each other. It may also be remarked here that the spectroscopic factors extracted from the comparison of the Coulomb breakup calculations of different models with the corresponding data could be quite different from each other, as has already been pointed out in [40].

IV. SUMMARY AND CONCLUSIONS

In this paper, we have studied the Coulomb and the nuclear breakup of the one-neutron halo nuclei, ^{11}Be and ^{19}C , on a ^{208}Pb target within a semiclassical fully dynamical model of the projectile excitation process. The time evolution of the projectile system is described by numerically solving the time dependent Schrödinger equation in three dimensions. Through this nonperturbative method higher order effects are fully taken into account in the breakup process. Unlike previous such calculations, we assume the projectile to move along a hyperbolic trajectory instead of a straight-line one. A simple single particle potential model was used to calculate the ground state wave function of the projectile nuclei.

With a configuration for the ^{11}Be ground state in which a $2s_{1/2}$ neutron is coupled to the ground state of the ^{10}Be core with a binding energy of 0.504 MeV and a spectroscopic factor of unity, the experimental relative energy distributions of the fragments (neutron and ^{10}Be) emitted in the breakup reaction of ^{11}Be on a lead target at the beam energy of 72 MeV/nucleon are described rather well by our model. The Coulomb breakup dominates these cross sections around the peak region while the nuclear breakup is important at higher relative energies. This provides a natural explanation for the failure of the pure Coulomb breakup calculations in describing these data at the larger relative energies.

For the ^{19}C case, the comparison of the dynamical calculations with the data for the relative energy spectrum of the fragments suggests that the ground state configuration of this nucleus is consistent with a $2s_{1/2}$ neutron coupled to the ground state of the ^{18}C core with a binding energy of 0.650 MeV and a spectroscopic factor of 1. Alternatively, it could also have a binding energy of 0.530 MeV but a spectroscopic factor of about 0.6 – 0.7. The current data [9] on the relative energy spectrum are not sufficient to rule out either of these possibilities. Further experimental studies in which the relative energy spectrum is measured by tagging the specific core states and calculations of the Coulomb and nuclear breakup effects within different models (e.g., finite range DWBA) are clearly needed to settle this issue.

By comparing the dynamical model results for the pure Coulomb breakup with the first order calculations (which are deduced from the same model in a particular limit), we find that higher order effects in these reactions are generally small. They reduce the magnitudes of the first order relative energy distribution of the fragments by about 10-15% in the peak region. Their shapes, however, remain almost unaltered by the higher order effects. However, a comparison of the higher order and first order calculations of two different models may lead to large differences in the two results. This is due to the fact that higher order calculations

performed within different theories include these effects in different approximations and could differ quite a bit from each other.

V. ACKNOWLEDGMENTS

One of us (R.S.) would like to thank Pawel Danielewicz for his kind hospitality in the theory group of the National Superconducting Cyclotron Laboratory at the Michigan State University. This work has been supported by the National Science Foundation grants No. PHY-0070818, PHY-0070911, and PHY-9528844.

- [1] P.G. Hansen and B. Jonson, *Europhys. Lett.* **4**, 409 (1987).
- [2] P.G. Hansen, A.S. Jensen, and B. Jonson, *Ann. Rev. Nucl. Part. Sci.* **45**, 2 (1995).
- [3] I. Tanihata, *J. Phys. G* **22**, 157 (1996), and references therein.
- [4] I. Tanihata *et al.*, *Phys. Lett.* **B206**, 592 (1988).
- [5] B. Blank *et al.*, *Z. Phys. A* **340**, 41 (1991).
- [6] M. Fukuda *et al.*, *Phys. Lett.* **B268**, 339 (1991).
- [7] D. Sackett *et al.*, *Phys. Rev. C* **48**, 118 (1993).
- [8] T. Nakamura *et al.*, *Phys. Lett.* **B331**, 296 (1994).
- [9] T. Nakamura *et al.*, *Phys. Rev. Lett.* **83**, 1112 (1999).
- [10] R. Chatterjee, P. Banerjee and R. Shyam, *Nucl. Phys.* **A675**, 477 (2000).
- [11] R. Anne *et al.*, *Phys. Lett.* **B250**, 19 (1990); **304**, 55 (1990).
- [12] F.M. Marqués *et al.*, *Phys. Lett.* **B381**, 407 (1996).
- [13] C.A. Bertulani and K.W. McVoy, *Phys. Rev. C* **46**, 2638 (1992).
- [14] N.A. Orr *et al.*, *Phys. Rev. C* **51**, 3116 (1995).
- [15] J.H. Kelley *et al.*, *Phys. Rev. Lett.* **74**, 30 (1995).
- [16] D. Bazin *et al.*, *Phys. Rev. Lett.* **74**, 3569 (1995); *Phys. Rev. C* **57**, 2156 (1998).
- [17] P. Banerjee and R. Shyam, *Phys. Lett.* **B349**, 421 (1995).
- [18] P.G. Hansen, *Phys. Rev. Lett.* **77**, 1016 (1996).
- [19] T. Baumann *et al.*, *Phys. Lett.* **B439**, 256 (1998).
- [20] R. Serber, *Phys. Rev.* **72**, 1016 (1947).
- [21] R. Shyam and P. Danielewicz, *Phys. Rev. C* **63**, 054608 (2001).
- [22] C.A. Bertulani and G. Baur, *Nucl. Phys.* **A480**, 615 (1988); M.S. Hussein, M.P. Pato and C. A. Bertulani, *Phys. Rev. C* **44**, 2219 (1991).
- [23] G.F. Bertsch and H. Esbensen, *Ann. Phys. (N.Y.)* **209**, 327 (1991); H. Esbensen and G.F. Bertsch, *Nucl. Phys.* **A542**, 310 (1992).
- [24] G. Baur and H. Rebel, *J. Phys. G: Nucl. Part. Phys.* **20**, 1 (1994); *Annu. Rev. Nucl. Part. Sci.* **46**, 321 (1997).
- [25] R. Anne *et al.*, *Nucl. Phys.* **A575**, 125 (1994).
- [26] F. Barranco, E. Vigenzzi, and R.A. Broglia, *Z. Phys.* **A356**, 45 (1996).
- [27] G. Baur, S. Typel, and H. Wolter, *Spins in Nuclear and Hadronic Reactions*, Proceedings of

- the RCNP-TAMU Symposium, edited by H. Yabu, T. Suzuki and H. Toki, World Scientific, Singapore (2000), page 119.
- [28] G. Baur, F. Rösler, D. Trautmann and R. Shyam, Phys. Rep. **111**, 333 (1984).
 - [29] A. Bonaccorso and D.M. Brink, Phys. Rev. C **38**, 1776 (1988); *ibid* Phys. Rev. C **57**, 2864 (1998), A. Bonaccorso, Phys. Rev. C **60**, 054604 (1999); A. Bonaccorso and F. Carstoiou, Phys. Rev. C **61**, 034605 (2000).
 - [30] K. Yabana, Y. Ogawa, and Y. Suzuki, Nucl. Phys. **A539**, 295 (1992).
 - [31] K. Henken, G.F. Bertsch, and H. Esbensen, Phys. Rev. C **54**, 3034 (1996); G.F. Bertsch, K. Henken, and H. Esbensen, Phys. Rev. C **57**, 1366 (1998); H. Esbensen and G. Bertsch, Phys. Rev. C **59**, 3240 (1999).
 - [32] C.A. Bertulani, G. Baur and M.S. Hussein, Nucl. Phys. **A526**, 751 (1991).
 - [33] R. Shyam and I.J. Thompson, Phys. Rev. C **59**, 2645 (1999).
 - [34] K. Alder and A. Winter, *Electromagnetic excitation* (North-Holland, Amsterdam, 1975).
 - [35] G.F. Bertsch and C.A. Bertulani, Nucl. Phys. **A556**, 136 (1993); C.A. Bertulani and G.F. Bertsch, Phys. Rev. C **49**, 2839 (1994).
 - [36] H. Esbensen, G.F. Bertsch and C. A. Bertulani, Nucl. Phys. **A581**, 107 (1995).
 - [37] T. Kido, K. Yabana and Y. Suzuki, Phys. Rev. C **53**, 2296 (1996).
 - [38] V.S. Melezhik and D. Baye, Phys. Rev. C **59**, 3232 (1999).
 - [39] J.A. Tostevin, Proceedings of the Second International Conference on Fission and Properties of neutron-Rich Nuclei, St. Andrews, Scotland, June 28 - July 2, 1999, edited by J. H. Hamilton, W. R. Phillips and H. K. Carter, World Scientific, Singapore (2000), 429.
 - [40] P. Banerjee and R. Shyam, Phys. Rev. C **61**, 047301 (2000).
 - [41] C.A. Bertulani and L.F. Canto, Nucl. Phys. **A539**, 163 (1992); L.F. Canto, R. Donangelo, A. Romanelli, and H. Schulz, Phys. Lett. **B318**, 415 (1993).
 - [42] S. Typel and G. Baur, Nucl. Phys. **A573**, 486 (1994); *ibid* Phys. Rev. C **50**, 2104 (1994); S. Typel, H.H. Wolter, and G. Baur, Nucl. Phys. **A613**, 147 (1997).
 - [43] S. Typel and H.H. Wolter, Z. Naturforsch. **54a**, 63 (1999).
 - [44] C.H. Dasso, S. M. Lenzi and A. Vitturi, Nucl. Phys. **A539**, 59 (1999); *ibid* Phys. Rec. C **59**, 539 (1999).
 - [45] E.K. Warburton and B.A. Brown, Phys. Rev. C **46**, 923 (1992).
 - [46] V. Maddalena *et al.*, Phys. Rev. C **63**, 24613 (2001).
 - [47] J. Wouters *et al.*, Z. Phys. A **331**, 229 (1988).
 - [48] N. Orr *et al.*, Phys. Lett. **B258**, 29 (1991).
 - [49] G. Audi and A.H. Wapstra, Nucl. Phys. **A565**, 1 (1993); G. Audi, O. Bersillon, J. Blachot, and A.H. Wapstra, Nucl. Phys. **A624**, 1 (1997).
 - [50] S. Typel and G. Baur, preprint nucl-th/0101033
 - [51] C.M. Perey and F.G. Perey, Atomic Data and Nuclear Data Tables **17**, 1 (1976)
 - [52] B. Bonin *et al.*, Nucl. Phys. **A445**, 381 (1985)
 - [53] M. Buenerd *et al.*, Nucl. Phys. **A424**, 313 (1984)